AGU PUBLICATIONS

Geophysical Research Letters

RESEARCH LETTER
10.1002/2017GL073309

Key Points:
- Calving front migration is responsible for 90% of Jakobshavn Isbrae's acceleration
- The acceleration is due to low basal drag in the trough and a viscosity feedback in the shear margins
- The glacier is likely to lose mass at a rate comparable to current for at least the next century

Supporting Information:
- Movie S1
- Movie S2
- Movie S3
- Supporting Information S1

Correspondence to:
J. H. Bondzio,
jbondzio@uci.edu

Citation:
Bondzio, J. H., M. Morlighem, H. Seroussi, T. Kleiner, M. Rückamp, J. Mouginot, T. Moon, E. Y. Larour, and A. Humbert (2017), The mechanisms behind Jakobshavn Isbræ's acceleration and mass loss: A 3-D thermomechanical model study, *Geophys. Res. Lett.*, *44*, 6252–6260, doi:10.1002/2017GL073309.

Received 3 MAR 2017
Accepted 31 MAY 2017
Accepted article online 2 JUN 2017
Published online 28 JUN 2017

The mechanisms behind Jakobshavn Isbræ's acceleration and mass loss: A 3-D thermomechanical model study

Johannes H. Bondzio[1,2], Mathieu Morlighem[1], Hélène Seroussi[3], Thomas Kleiner[2], Martin Rückamp[2], Jeremie Mouginot[1], Twila Moon[4], Eric Y. Larour[3], and Angelika Humbert[2,5]

[1]Department of Earth System Science, University of California, Irvine, California, USA, [2]Alfred-Wegener-Institute, Helmholtz-Centre for Polar and Marine Research, Bremerhaven, Germany, [3]Jet Propulsion Laboratory, California Institute of Technology, Pasadena, California, USA, [4]National Snow and Ice Data Center, University of Colorado Boulder, Boulder, Colorado, USA, [5]Faculty of Geosciences, University of Bremen, Bremen, Germany

Abstract The mechanisms causing widespread flow acceleration of Jakobshavn Isbræ, West Greenland, remain unclear despite an abundance of observations and modeling studies. Here we simulate the glacier's evolution from 1985 to 2016 using a three-dimensional thermomechanical ice flow model. The model captures the timing and 90% of the observed changes by forcing the calving front. Basal drag in the trough is low, and lateral drag balances the ice stream's driving stress. The calving front position is the dominant control on changes of Jakobshavn Isbræ since the ice viscosity in the shear margins instantaneously drops in response to the stress perturbation caused by calving front retreat, which allows for widespread flow acceleration. Gradual shear margin warming contributes 5 to 10% to the total acceleration. Our simulations suggest that the glacier will contribute to eustatic sea level rise at a rate comparable to or higher than at present.

1. Introduction

Jakobshavn Isbræ is the fastest marine-terminating outlet glacier of the Greenland Ice Sheet (GrIS) [*Rignot and Mouginot*, 2012]. The disintegration of its floating ice tongue between 1998 and 2004 triggered rapid calving front retreat, as well as widespread flow acceleration and mass loss [*Joughin et al.*, 2008; *Howat et al.*, 2011]. Since the disintegration, it has been contributing to eustatic sea level rise at an increasing rate, reaching about 0.1 mm yr^{-1} in 2011 [*Howat et al.*, 2011]. The mechanisms that sustain the acceleration remain unclear despite an abundance of observations [e.g., *Csatho et al.*, 2008; *Joughin et al.*, 2008, 2014] and modeling studies [e.g., *Truffer and Echelmeyer*, 2003; *Thomas*, 2004; *van der Veen et al.*, 2011; *Joughin et al.*, 2012]. Many marine-terminating outlet glaciers of the GrIS are undergoing similar dynamic changes [*Moon et al.*, 2014], which are therefore crucial to understand in order to provide reliable projections of the GrIS's future contribution to eustatic sea level rise.

Jakobshavn Isbræ discharges ice into the ocean through two branches (Figure 1a) that disconnected in 2004 [*Joughin et al.*, 2008]. The main branch, commonly referred to as "ice stream" [*Cuffey and Paterson*, 2010] and as JI in this text, flows significantly faster than the northern branch, and is located in a deep (−1700 m below sea level) and narrow (about 5–6 km wide) trough (Figure 1b) [*Gogineni et al.*, 2014; *Morlighem et al.*, 2014]. Pronounced shear margins exert a strong control on the flow regime and characterize JI [e.g., *Truffer and Echelmeyer*, 2003].

Three hypotheses have been proposed to explain the speedup of JI. The first hypothesis (H1) suggests that thinning of the ice tongue and retreat of the calving front cause a back force reduction, which is swiftly transmitted upstream through an unknown mechanism, leading to widespread ice flow acceleration [*Thomas*, 2004]. The second hypothesis (H2) proposes that the inland flow acceleration is a response to shear margin weakening corresponding to a local viscosity drop of over 60%, caused by an uncertain process [*van der Veen et al.*, 2011]. The third hypothesis (H3) argues that dynamic-thinning-induced feedbacks and basal hydrological processes following the disintegration both increased the driving stress and decreased the basal drag of the ice stream causing sustained acceleration inland [*Vieli and Nick*, 2011; *Joughin et al.*, 2012].

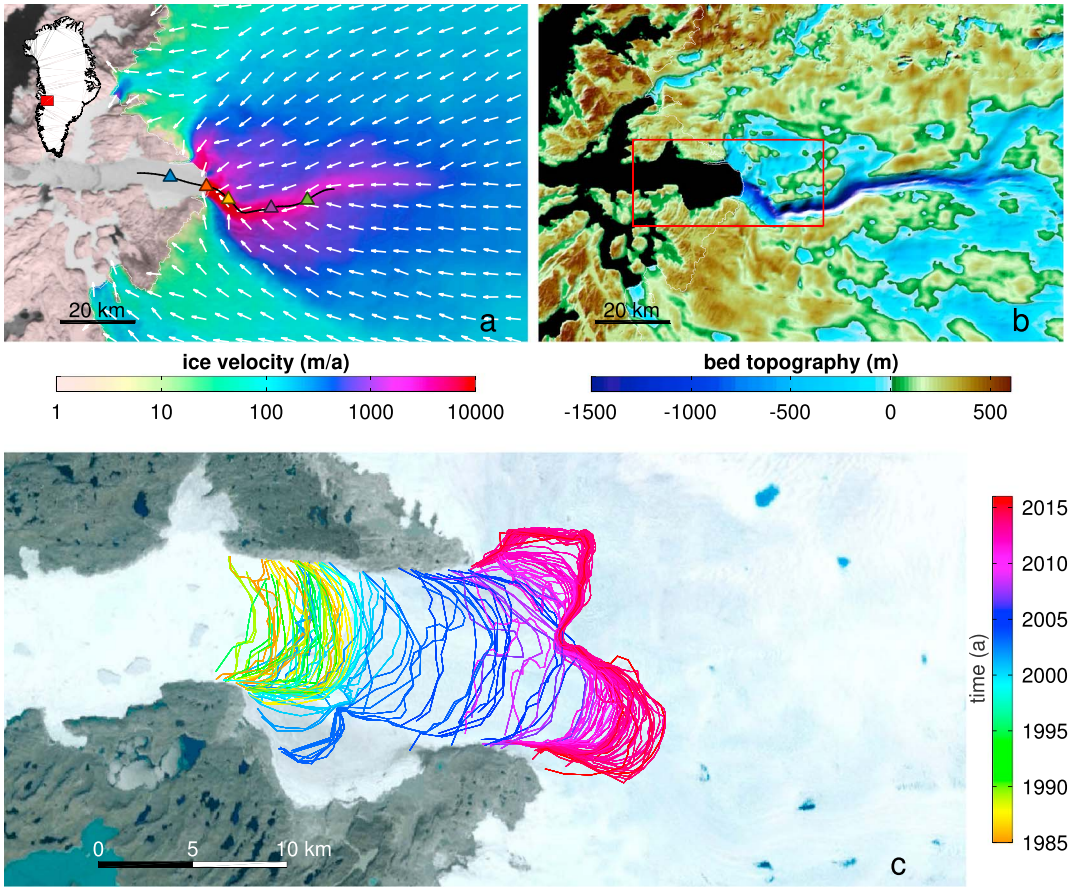

Figure 1. State and evolution of JI. (a) Observed surface flow velocities (2008–2009, logarithmic scale [*Rignot and Mouginot*, 2012]). White arrows show the flow direction. The calving front evolution in Figure 2a is tracked along the black flow line. Colored triangles denote the locations for velocity comparison in Figure 2b. (b) Bedrock topography in the same region, shaded relief [*Morlighem et al.*, 2014]. (c) Observed calving front positions of JI from 1985 until end of 2015, derived from Landsat 5–8, ERS-1 and 2, and TerraSAR-X satellite imagery. Location of Figure 1c is shown by red inset in Figure 1b. Satellite background image: Landsat 7 (1 July 2001)© Google Earth.

These three hypotheses were derived using models that did not include certain important processes, relied on coarse-resolution observations, and led to different conclusions, underlining that the mechanisms at play are not fully understood. Recent developments in ice flow modeling, including moving boundary capabilities in ice sheet models [*Bondzio et al.*, 2016] and the new availability of high-resolution model input data [*Joughin et al.*, 2014; *Morlighem et al.*, 2014; *Howat et al.*, 2014; *Noël et al.*, 2015], make it possible to overcome these shortcomings and to provide a more complete analysis. Here we investigate the mechanisms that sustain the glacier's ongoing acceleration and mass loss using high-resolution input data and a migrating calving front in the Ice Sheet System Model (ISSM) [*Larour et al.*, 2012], a state-of-the-art, finite element ice flow model.

2. Ice Flow Model

We compute the ice velocities using the Higher-Order Model [*Blatter*, 1995; *Pattyn*, 2003]. We use a linear viscous basal friction law (supporting information (SI)); equation (1) [*Budd et al.*, 1984] and assume that ice deformation follows a nonlinear, isotropic flow law [*Glen*, 1955; *Nye*, 1957] with a stress exponent $n = 3$. We compute the ice viscosity, μ, as

$$\mu = (1 - D)\frac{B(T, w)}{2\dot{\varepsilon}_e^{\frac{n-1}{n}}}. \quad (1)$$

Here $\dot{\varepsilon}_e$ is the effective strain rate, and the ice viscosity parameter, B, depends on the ice temperature, T, and the microscopic water content, w [*Cuffey and Paterson*, 2010; *Lliboutry and Duval*, 1985]. A damage parameter

field D softens the ice in the shear margins [*Borstad et al.*, 2012]. It is 0.3 near the grounding line and drops linearly to 0 (no damage) at 70 km distance inland and stays constant in time. The grounding line evolves based on hydrostatic equilibrium following a subelement migration scheme [*Seroussi et al.*, 2014]. We model the thermal regime using an energy-conserving enthalpy formulation [*Aschwanden et al.*, 2012; *Seroussi et al.*, 2013; *Kleiner et al.*, 2015], and we track the calving front position using a level set method [*Bondzio et al.*, 2016] that has been extended from two horizontal dimensions to three dimensions (3-D) for this study, by assuming that the calving front remains vertical throughout the simulation. The model does not account for basal hydrology nor cryohydrological warming [*Phillips et al.*, 2010].

3. Model and Experiment Setup

We set up a 3-D thermomechanical model of Jakobshavn Isbræ in 1985, calibrated using available data sets (SI, Text S1). We mesh the glacier's drainage basin [*Rignot and Mouginot*, 2012] with a horizontal resolution of 400 m in regions of high strain rates and steep bedrock slopes, and up to 4 km elsewhere. The horizontal mesh is vertically extruded into 17 layers that are more closely spaced toward the base. The resulting mesh consists of about 675,000 prismatic P1 × P1 elements. We use a time step of about 1 day.

We simulate Jakobshavn Isbræ's evolution from 1 January 1985 until 31 December 2015. Along the lateral boundary, except the calving front, we prescribe observed surface velocities [*Rignot and Mouginot*, 2012], as well as ice temperatures from a thermomechanical simulation of the GrIS [*Seroussi et al.*, 2013]. At the ice surface, we impose annual average surface temperatures and annual cumulative surface mass balance from RACMO2.3 [*Noël et al.*, 2015]. At the ice base, we prescribe the geothermal heat flux by *Shapiro and Ritzwoller* [2004], and the basal boundary conditions of the enthalpy method adjust dynamically to the thermal state of the base [*Aschwanden et al.*, 2012, Figure 5]. The basal friction coefficient field, inferred from 1985 conditions, is kept fixed throughout the simulations. The submarine melting rate under floating ice is modeled as a piecewise linear function of depth [cf. *Favier et al.*, 2014]. We impose an ice tongue-averaged melting rate of 350 m yr^{-1} until 1990, 270 m yr^{-1} from 1990 through 1995, and 540 m yr^{-1} from 1996 onward in order to account for observed changes in ambient ocean temperatures [*Holland et al.*, 2008; *Motyka et al.*, 2011; *Enderlin and Howat*, 2013].

We force the calving front position explicitly from over 500 observations (Figure 1c), which have been compiled from Landsat 5–8, ERS-1 and 2, and TerraSAR-X satellite scenes [cf. *Moon et al.*, 2014]. We interpolate this forcing linearly in the time between two observations. All other forcings and boundary conditions are kept constant.

4. Results

The calving front retreat from 1998 onward triggers strong flow acceleration and mass loss in the model, which is in close agreement with observations (Figure 2). Annual average ice velocities double until 2011 along the entire ice stream (Figure 2b and SI, Figure S3). Ice velocities develop a growing seasonal variability of 20 to 40% of the annual average velocity in regions of fast flow, which is most pronounced close to the calving front (Figure 2b). The highest seasonal ice velocities occur during rapid retreat when the terminus is grounded (cf. SI, Movie S1). Basal sliding contributes between 60 and 100% to the modeled motion of JI. Prior to the disintegration of the ice tongue, the glacier loses about 5.5 Gt of ice per year (Figure 2c). This rate of mass loss rapidly increases afterward, reaching an average value of 34.1 Gt yr^{-1} from 2004 onward (Figure 2c). A sensitivity analysis (SI, Figure S4) shows that these results depend weakly on the prescribed submarine melting rate, and only if a floating ice tongue is present. Model simulations with a fixed calving front position show no seasonal variation (SI, Figure S5).

Both the timing and amplitude of summer and winter velocities are in good agreement with observations (Figure 3a). Prior to the ice tongue's disintegration, the ratio of modeled to observed ice surface velocities ranges between 90 and 110%. During and after the disintegration, this ratio decreases to about 80 to 90%. The highest deviations (>20%) occur at locations closest to the calving front, where ice velocities are sensitive to the exact calving front position, the grounding line position, the bedrock topography, and errors thereof. The strongly subdued seasonal signal in the velocity ratio shows that the model reproduces the timing of the seasonal velocity variation accurately along the entire ice stream.

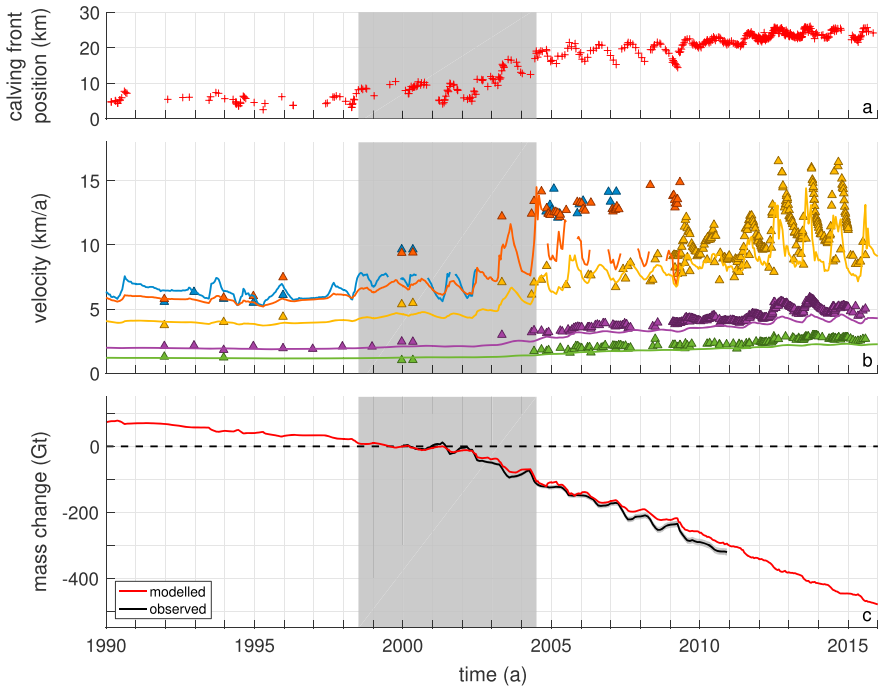

Figure 2. Comparison of observations and model results. (a) Calving front positions from satellite observations along the flow line in Figure 1a. (b) Comparison of observed velocities (triangles) and modeled velocities (lines). Colors correspond to the triangle locations shown in Figure 1a. Lines are discontinuous when the calving front retreats upstream of the corresponding location. (c) JI's modeled mass change (red line) relative to 1 January 2000. The black line with error envelope shows observed mass changes [*Howat et al.*, 2011], and the black dashed line represents volume preservation. The grey boxes mark the period of ice tongue disintegration.

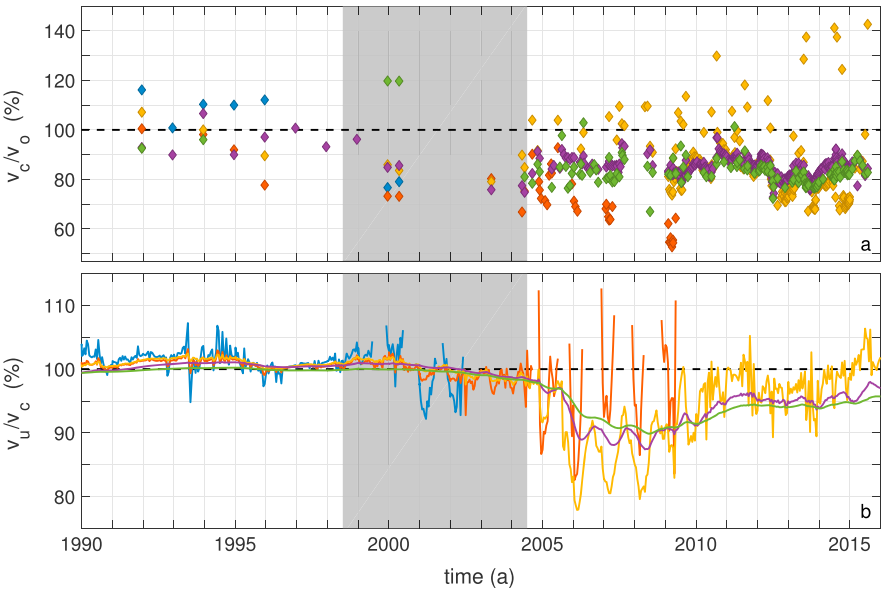

Figure 3. Comparison of modeled and observed surface ice flow velocities. (a) Ratio of thermomechanically coupled (v_c) and observed ice surface velocities (v_o). (b) Ratio of modeled ice surface velocities without (v_u) and with (v_c) thermomechanical coupling. The black dashed lines represent exact matching of the considered velocity values. Marker and line colors correspond to the colors of the triangles in Figure 1a. Lines are discontinuous when the calving front retreats upstream of the corresponding location. The gray patches mark the time of the ice tongue disintegration.

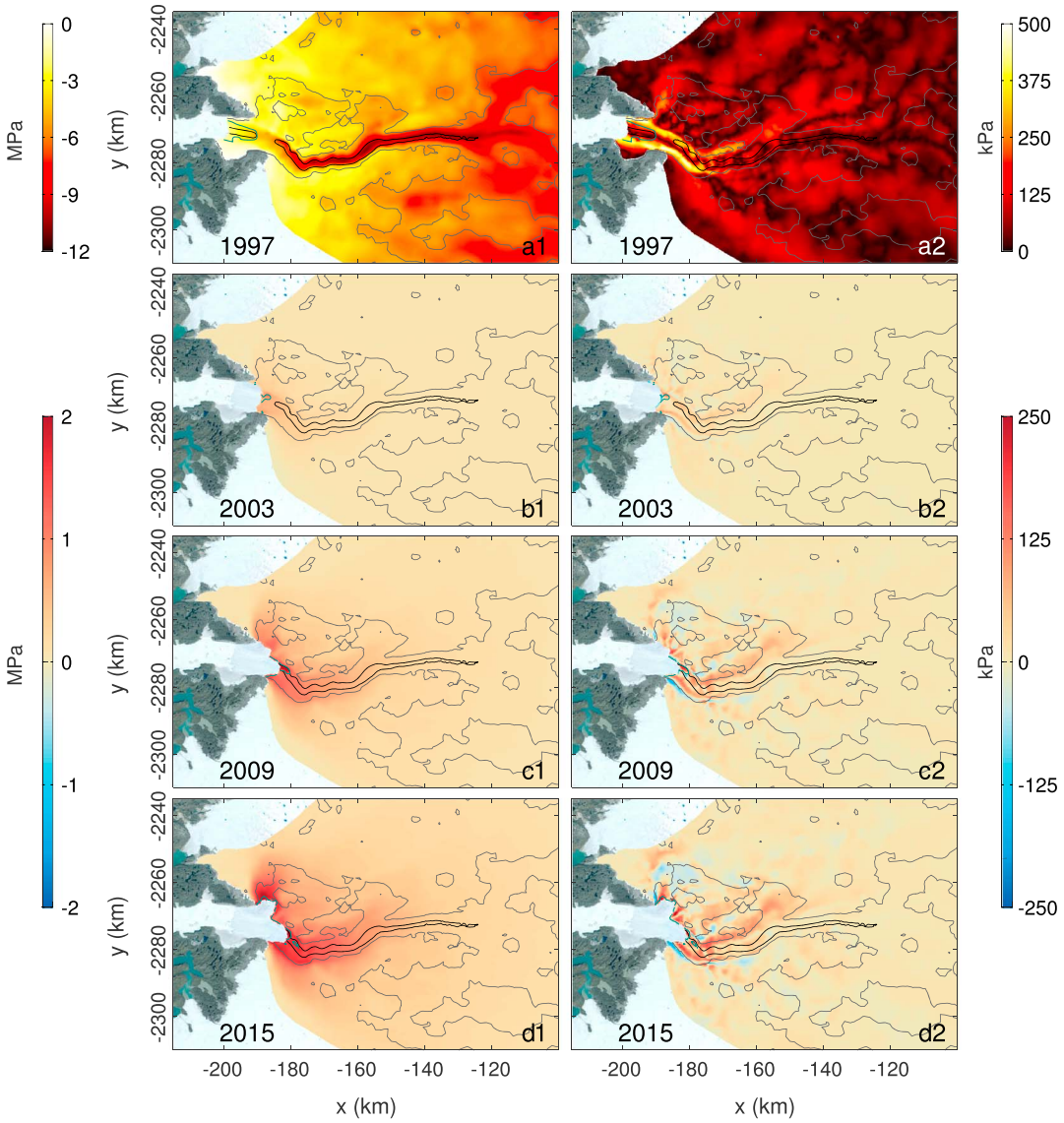

Figure 4. Evolution of the modeled stress regime. Left column: depth-averaged longitudinal stress. The negative sign denotes compressive stress. (a1) Annual average in 1997. (b1, c1, d1) Change compared to 1997 in indicated years. Right column: magnitude of the depth-averaged lateral stress. (a2) Annual average in 1997. (b2, c2, d2) Change compared to 1997 in indicated years. Grey and black lines denote bedrock contours at 0 and −1000 m elevation, respectively. The green line denotes the average modeled grounding line position for each year. Satellite background image: Landsat 7 (1 July 2001)© Google Earth.

After the disintegration of the ice tongue, ice velocities of a thermomechanically coupled model simulation exceed those of an uncoupled model in which the enthalpy is kept constant (Figure 3b). Prior to and during the disintegration, the respective ice velocities agree within 1 to 2%. However, the ice velocities of the coupled model rapidly increase relative to the ones of the uncoupled model by an average of 10% from the end of the disintegration onward. Their ratio develops a strong seasonal signal that is strongest near the terminus and decreases to about 5% after 2009. The higher flow velocities of the coupled model and its stronger mass loss are in better agreement with observations (SI, Figures S4 and S6).

We analyze the glacier's stress balance in a coordinate system that has been rotated along flow and distinguish the two horizontal directions as "longitudinal" (along flow) and "lateral" (across flow). Compressive longitudinal stress of up to −12 MPa resists ice flow in JI's deep trough (Figure 4a1). There, basal drag is low (1 kPa), and lateral stress (up to 570 kPa per unit depth) transfers most of the ice stream's driving stress to the adjacent trough walls and bedrock (Figure 4a2 and SI, Figures S7a and S8a). The calving front retreat and ensuing

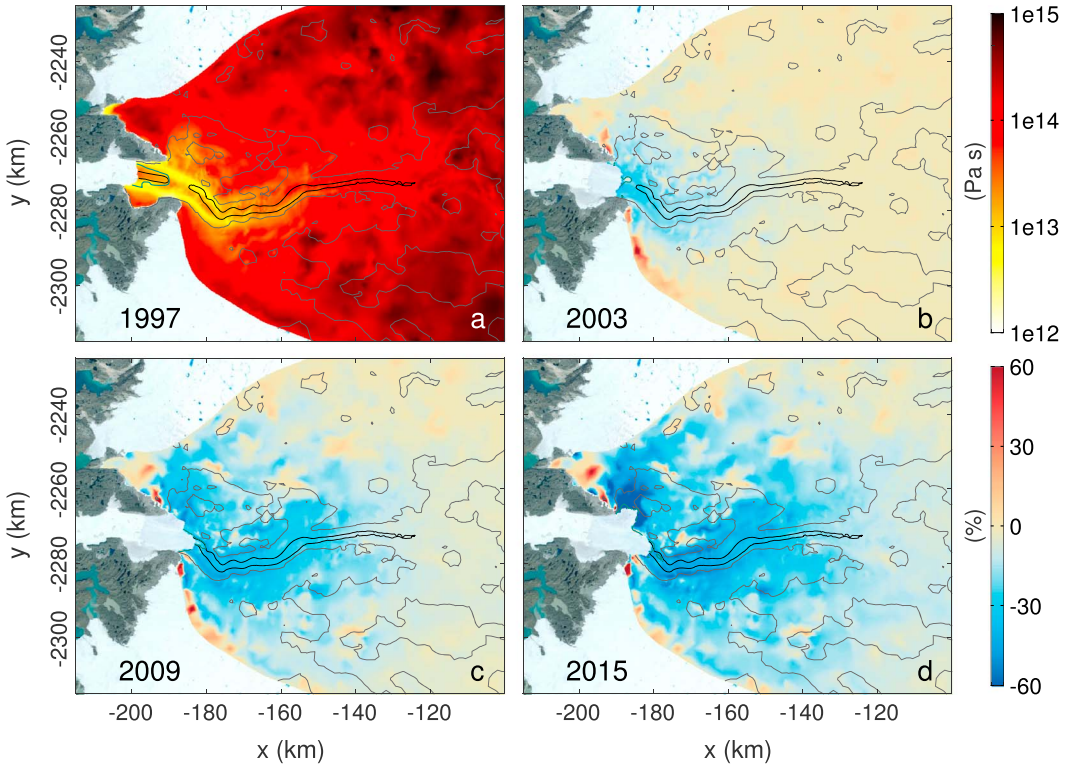

Figure 5. Evolution of Jakobshavn Isbræ's depth-averaged ice viscosity. (a) Annual average in 1997 (top color bar). (b–d) Change compared to 1997 in indicated years (bottom color bar). Grey and black lines denote bedrock contours at 0 and −1000 m elevation, respectively. The green line denotes the average modeled grounding line position for each year. Satellite background image: Landsat 7 (1 July 2001)© Google Earth.

dynamic thinning decreases the back stress along the lowermost 40 to 50 km of the ice stream by up to 2 MPa (Figures 4b1, 4c1, and 4d1 and SI, Figure S9). The ice stream's driving stress increases by up to 150 kPa through surface steepening (SI, Figure S7). Lateral stress transfer increases by 85 to 230 kPa to balance the stress perturbation caused by calving front retreat (Figures 4b2, 4c2, and 4d2).

JI's depth-averaged ice viscosity varies over 4 orders of magnitude, from 2.42×10^{16} Pa s inland down to 1.51×10^{12} Pa s in the shear margins (Figure 5a). The soft ice in the shear margins allows for high flow velocities in the ice stream. The annual average ice viscosity decreases gradually by 20% to more than 60% during the calving front retreat (Figures 5b–5d). The largest viscosity drop occurs in the shear margins and near the calving front once the ice tongue has disintegrated due to the increase in effective strain rate. The viscosity drop originates from the calving front, instantaneously spreads along the ice stream in a linearly dampened fashion, and diffuses from there to the surrounding ice sheet (cf. SI, Movie S2). Enhanced strain heating following the disintegration warms the shear margins by up to 2°C (cf. SI, Figures S10b–S10d), which contributes 20 to 30% to the total viscosity drop.

5. Discussion

The combination of low basal drag in the trough under JI and the nonlinear rheology of ice creates a stress regime that is highly susceptible to stress perturbations, caused, e.g., by calving front retreat, and allows for widespread inland acceleration. In agreement with earlier studies [*Thomas*, 2004; *Joughin et al.*, 2012; *Shapero et al.*, 2016], basal drag in the center of the ice stream is 1 to 2 orders of magnitude lower than the driving stress, which therefore has to be transferred laterally to the adjacent steep trough walls. This creates pronounced shear margins with low ice viscosity that allow for fast ice flow (cf. Figure 5 and SI, Figure S11). The combination of the trough's low basal drag and soft shear margins allows to swiftly transfer stress perturbations originating from the calving front tens of kilometers inland through longitudinal stress. Calving front retreat triggers an instantaneous positive feedback upstream. The ice viscosity is a function of the effective strain rate, the temperature, and microscopic water content (equation (1)). Any increase in effective strain rate

thus softens the inland ice, which in turn allows for higher strain rates, higher strain heating, and even faster flow. Ensuing dynamic thinning steepens the areas surrounding the ice stream, which increases the driving stress inland, and the softened ice readjusts rapidly to the new geometric configuration (cf. SI, Figures S7 and S12). Hence, calving front retreat is able to trigger widespread inland acceleration, and JI's calving rates are currently the main control on its change.

The thermal regime of the glacier is advection dominated (cf. SI, Figures S10a and S13 and Movie S3). Enhanced strain heating gradually softens the shear margins during continued calving front retreat, so that ice flow velocities of a thermomechanical simulation are higher than those of an uncoupled simulation after the disintegration of the ice tongue. We conclude that accounting for the thermal regime is important in simulations of rapidly changing glaciers.

The model studies from which H1, H2, and H3 have been derived were designed to investigate different aspects of the mechanism interplay during calving front retreat and therefore came to different conclusions. Our results support H1 and reveal the lacking mechanism through which the stress perturbation caused by calving front retreat is transferred inland. In agreement with H2, shear margin weakening allows for widespread inland flow acceleration. However, the shear margin weakening is a response to the calving front retreat and not the initial trigger for the acceleration. Corroborating H3, thinning-induced driving stress increase through surface steepening contributes to the flow acceleration inland, where basal drag is higher. The initial viscosity drop facilitates the geometrical adjustment. Thinning-induced grounding line retreat and the drop in effective basal pressure affect the glacier flow only in the lowest 8 to 10 km upstream of the grounding line, in agreement with *Joughin et al.* [2012] and *Habermann et al.* [2013].

The model accurately reproduces the timing and amplitude of the observed seasonal flow signal when forced only with the observed calving front position. Therefore, we conclude that the viscosity drop, the trough's low basal drag, and the geometrical adjustment are the main drivers behind the observed inland acceleration of JI. Physical processes such as major variations in basal hydrology [*Joughin et al.*, 2012; *Lampkin et al.*, 2013], sudden englacial warming [*van der Veen et al.*, 2011], cryohydrological warming [*Phillips et al.*, 2010], and development of englacial damage are not necessary to explain the extent and amplitude of JI's observed velocities.

Several factors cause the 10% underestimation of flow velocities in the model. For technical reasons, the calving front position in the model is displaced up to one finite element width downstream of the observed position [*Bondzio et al.*, 2016]. This systematically increases the back stress in the model, especially after the disintegration of the ice tongue when the terminus is often grounded and the ice stream is highly sensitive to the calving front position, the bedrock topography, and errors thereof. The underestimation of the inland acceleration may be caused by uncertainties in the basal sliding law and in the applied material law. The material law does not extend to microscopic water values larger than 1%. However, water content values up to 3% are found throughout the lower drainage basin of the model in a thick basal temperate layer, and significant ice warming occurs at the ice base in response to the flow acceleration (SI, Movie S3). Moreover, a larger value of the stress exponent, n, will allow for larger seasonal velocity variation.

Deep troughs with low basal drag are a common feature under many marine-terminating outlet glaciers of the GrIS [*Morlighem et al.*, 2014; *Shapero et al.*, 2016], and we expect that the mechanisms described here apply to these glaciers as well. It is therefore critical to explicitly account for the interplay of the lateral stress transfer through shear margins, the thermal regime, and the migrating calving front in model simulations of this type of glaciers. This makes flow line and flow band models unsuitable for producing realistic projections of future eustatic sea level rise of the GrIS [*Nick et al.*, 2009; *Vieli and Nick*, 2011; *Nick et al.*, 2013]. Moreover, realistic projections will require a better material law for temperate glacier ice, better understanding of basal processes, and a calving rate parameterization that is suitable for continental-scale ice sheet models.

The proposed mechanisms for glacier acceleration imply that JI will continue to retreat and lose mass. Air and ocean temperatures, ice mélange rigidity, strain rates, and bedrock topography are major controls on JI's calving rates [*Sohn et al.*, 1998; *Benn et al.*, 2007; *Joughin et al.*, 2008; *Alley et al.*, 2008; *Amundson et al.*, 2010; *Cassotto et al.*, 2015; *Morlighem et al.*, 2016]. Ongoing climate warming will further weaken the ice mélange, and strain rates will remain high while the glacier adjusts to the retreated calving front position. We argue therefore that the glacier will not readvance in the coming years to decades. Under the most conservative assumption of calving front stabilization at the current position, additional model simulations show that the

glacier would contribute 2.77 ± 0.78 mm to eustatic sea level rise until 2100 due to ongoing geometry adjustment to the retreated calving front position (cf. SI, Figure S14). However, the observed calving front positions over the past three decades and model studies show that rapid retreat occurs over overdeepened bedrock topography (Figure 1c) [*Joughin et al.*, 2014; *Morlighem et al.*, 2016], which characterizes most of JI's trough for the 60 to 70 km upstream of the 2016 calving front position. Therefore, we find the scenario of continued intermittent calving front retreat significantly more likely, in agreement with *Joughin et al.* [2012]. This scenario represents a commitment to eustatic sea level rise from JI for at least the next several decades at a rate comparable to or higher than today.

6. Conclusions

In this study, we model the dynamic evolution of Jakobshavn Isbræ using a 3-D thermomechanical ice flow model, whose only seasonal forcing is the calving front position imposed from observations. The model reproduces about 80 to 90% of the observed widespread acceleration, its seasonal timing, the observed mass loss, and the glacier's thermal regime.

Low basal drag in the center of the lowermost 40 to 50 km of JI's deep trough creates a stress regime where most of the driving stress is balanced laterally by the trough walls. The stress regime is highly sensitive to calving front retreat, since the corresponding stress perturbation causes the ice viscosity to drop instantaneously, which decreases lateral drag. The stress perturbation is therefore only weakly dampened along flow and is able to cause widespread flow acceleration and dynamic thinning. Shear margin warming through enhanced strain rates after the disintegration of the ice tongue contributes 5 to 10% to the total acceleration. Geometrical adjustment to the dynamically thinning ice stream spreads the acceleration inland, which is facilitated by the lowered ice viscosity. These mechanisms are likely to apply to many other marine-terminating outlet glaciers of the GrIS, and the interplay of calving front migration, shear margins, and the thermal regime is important to account for in projections of future eustatic sea level rise. Our simulations suggest that the glacier will continue to contribute to eustatic sea level rise for at least the next several decades at a rate comparable to or higher than at present.

Acknowledgments
This work was performed at the University of California Irvine under a contract with the National Aeronautics and Space Administration, Cryospheric Sciences Program (NNX15AD55G). We thank R. Rosenau for providing digitized calving front positions of JI. We thank the Editor and the reviewers for the fruitful discussion. The authors declare that they have no competing financial interests.

References

Alley, R., H. Horgan, I. Joughin, K. Cuffey, T. Dupont, B. Parizek, S. Anandakrishnan, and J. Bassis (2008), A simple law for ice-shelf calving, *Science*, *322*(5906), 1344.

Amundson, J. M., M. Fahnestock, M. Truffer, J. Brown, M. P. Lüthi, and R. J. Motyka (2010), Ice mélange dynamics and implications for terminus stability, Jakobshavn Isbræ, Greenland, *J. Geophys. Res.*, *115*, F01005, doi:10.1029/2009JF001405.

Aschwanden, A., E. Bueler, C. Khroulev, and H. Blatter (2012), An enthalpy formulation for glaciers and ice sheets, *J. Glaciol.*, *58*(209), 441–457, doi:10.3189/2012JoG11J088.

Benn, D. I., C. R. Warren, and R. H. Mottram (2007), Calving processes and the dynamics of calving glaciers, *Earth Sci. Rev.*, *82*(3–4), 143–179, doi:10.1016/j.earscirev.2007.02.002.

Blatter, H. (1995), Velocity and stress-fields in grounded glaciers: A simple algorithm for including deviatoric stress gradients, *J. Glaciol.*, *41*(138), 333–344.

Bondzio, J. H., H. Seroussi, M. Morlighem, T. Kleiner, M. Rückamp, A. Humbert, and E. Larour (2016), Modelling calving front dynamics using a level-set method: Application to Jakobshavn Isbræ, West Greenland, *Cryosphere*, *10*(2), 497–510, doi:10.5194/tc-10-497-2016.

Borstad, C. P., A. Khazendar, E. Larour, M. Morlighem, E. Rignot, M. P. Schodlok, and H. Seroussi (2012), A damage mechanics assessment of the Larsen B ice shelf prior to collapse: Toward a physically-based calving law, *Geophys. Res. Lett.*, *39*, L18502, doi:10.1029/2012GL053317.

Budd, W., D. Jenssen, and I. Smith (1984), A three-dimensional time-dependent model of the West Antarctic ice-sheet, *Ann. Glaciol.*, *5*, 29–36.

Cassotto, R., M. Fahnestock, J. M. Amundson, M. Truffer, and I. Joughin (2015), Seasonal and interannual variations in ice melange and its impact on terminus stability, Jakobshavn Isbræ, Greenland, *J. Glaciol.*, *61*(225), 76–88, doi:10.3189/2015JoG13J235.

Csatho, B., T. Schenk, C. J. Van Der Veen, and W. B. Krabill (2008), Intermittent thinning of Jakobshavn Isbrae, West Greenland, since the Little Ice Age, *J. Glaciol.*, *54*(184), 131–144, doi:10.3189/002214308784409035.

Cuffey, K., and W. S. B. Paterson (2010), *The Physics of Glaciers*, 4th ed., Elsevier, Oxford, U. K.

Enderlin, E. M., and I. M. Howat (2013), Submarine melt rate estimates for floating termini of Greenland outlet glaciers (2000-2010, *J. Glaciol.*, *59*(213), 67–75, doi:10.3189/2013JoG12J049.

Favier, L., G. Durand, S. L. Cornford, G. H. Gudmundsson, O. Gagliardini, F. Gillet-Chaulet, T. Zwinger, A. J. Payne, and A. Le Brocq (2014), Retreat of Pine Island Glacier controlled by marine ice-sheet instability, *Nat. Clim. Change*, *4*, 117–121, doi:10.1038/NCLIMATE2094.

Glen, J. (1955), The creep of polycrystalline ice, *Proc. R. Soc. A*, *228*(1175), 519–538.

Gogineni, S., et al. (2014), Bed topography of Jakobshavn Isbrae, Greenland, and Byrd Glacier, Antarctica, *J. Glaciol.*, *60*(223), 813–833, doi:10.3189/2014JoG14J129.

Habermann, M., M. Truffer, and D. Maxwell (2013), Changing basal conditions during the speed-up of Jakobshavn Isbræ, Greenland, *Cryosphere*, *7*(6), 1679–1692, doi:10.5194/tc-7-1679-2013.

Holland, D., R. Thomas, B. De Young, M. Ribergaard, and B. Lyberth (2008), Acceleration of Jakobshavn Isbrae triggered by warm subsurface ocean waters, *Nat. Geosci.*, *1*(10), 659–664, doi:10.1038/ngeo316.

Howat, I. M., Y. Ahn, I. Joughin, M. R. van den Broeke, J. T. M. Lenaerts, and B. Smith (2011), Mass balance of Greenland's three largest outlet glaciers, 2000–2010, *Geophys. Res. Lett.*, *38*, L12501, doi:10.1029/2011GL047565.

Howat, I. M., A. Negrete, and B. E. Smith (2014), The Greenland Ice Mapping Project (GIMP) land classification and surface elevation datasets, *Cryosphere*, *8*(4), 1509–1518, doi:10.5194/tc-8-1509-2014.

Joughin, I., B. E. Smith, I. M. Howat, D. Floricioiu, R. B. Alley, M. Truffer, and M. Fahnestock (2012), Seasonal to decadal scale variations in the surface velocity of Jakobshavn Isbrae, Greenland: Observation and model-based analysis, *J. Geophys. Res.*, *117*, F02030, doi:10.1029/2011JF002110.

Joughin, I., I. M. Howat, M. Fahnestock, B. Smith, W. Krabill, R. B. Alley, H. Stern, and M. Truffer (2008), Continued evolution of Jakobshavn Isbrae following its rapid speedup, *J. Geophys. Res.*, *113*, F04006, doi:10.1029/2008JF001023.

Joughin, I., B. E. Smith, D. E. Shean, and D. Floricioiu (2014), Brief communication: Further summer speedup of Jakobshavn Isbræ, *Cryosphere*, *8*(1), 209–214, doi:10.5194/tc-8-209-2014.

Kleiner, T., M. Rückamp, J. Bondzio, and A. Humbert (2015), Enthalpy benchmark experiments for numerical ice sheet models, *Cryosphere*, *9*, 217–228, doi:10.5194/tc-9-217-2015.

Lampkin, D. J., N. Amador, B. R. Parizek, K. Farness, and K. Jezek (2013), Drainage from water-filled crevasses along the margins of Jakobshavn Isbræ: A potential catalyst for catchment expansion, *J. Geophys. Res. Earth Surf.*, *118*, 795–813, doi:10.1002/jgrf.20039.

Larour, E., H. Seroussi, M. Morlighem, and E. Rignot (2012), Continental scale, high order, high spatial resolution, ice sheet modeling using the Ice Sheet System Model (ISSM), *J. Geophys. Res.*, *117*, F01022, doi:10.1029/2011JF002140.

Lliboutry, L. A., and P. Duval (1985), Various isotropic and anisotropic ices found in glaciers and polar ice caps and their corresponding rheologies, *Ann. Geophys.*, *3*, 207–224.

Moon, T., I. Joughin, B. Smith, M. R. van den Broeke, W. J. van de Berg, B. Noel, and M. Usher (2014), Distinct patterns of seasonal Greenland glacier velocity, *Geophys. Res. Lett.*, *41*, 7209–7216, doi:10.1002/2014GL061836.

Morlighem, M., E. Rignot, J. Mouginot, H. Seroussi, and E. Larour (2014), Deeply incised submarine glacial valleys beneath the Greenland Ice Sheet, *Nat. Geosci.*, *7*(6), 418–422, doi:10.1038/ngeo2167.

Morlighem, M., J. Bondzio, H. Seroussi, E. Rignot, E. Larour, A. Humbert, and S.-A. Rebuffi (2016), Modeling of Store Gletscher's calving dynamics, West Greenland, in response to ocean thermal forcing, *Geophys. Res. Lett.*, *43*, 2659–2666, doi:10.1002/2016GL067695.

Motyka, R. J., M. Truffer, M. Fahnestock, J. Mortensen, S. Rysgaard, and I. Howat (2011), Submarine melting of the 1985 Jakobshavn Isbrae floating tongue and the triggering of the current retreat, *J. Geophys. Res.*, *116*, F01007, doi:10.1029/2009JF001632.

Nick, F. M., A. Vieli, I. M. Howat, and I. Joughin (2009), Large-scale changes in Greenland outlet glacier dynamics triggered at the terminus, *Nat. Geosci.*, *2*(2), 110–114, doi:10.1038/NGEO394.

Nick, F. M., A. Vieli, M. L. Andersen, I. Joughin, A. Payne, T. L. Edwards, F. Pattyn, and R. S. W. van de Wal (2013), Future sea-level rise from Greenland's main outlet glaciers in a warming climate, *Nature*, *497*(7448), 235–238.

Noël, B., W. J. van de Berg, E. van Meijgaard, P. K. Munneke, R. S. W. van de Wal, and M. R. van den Broeke (2015), Evaluation of the updated regional climate model RACMO2.3: Summer snowfall impact on the Greenland Ice Sheet, *Cryosphere*, *9*(5), 1831–1844, doi:10.5194/tc-9-1831-2015.

Nye, J. (1957), The distribution of stress and velocity in glaciers and ice-sheets, *Proc. R. Soc. A*, *239*(1216), 113–133.

Pattyn, F. (2003), A new three-dimensional higher-order thermomechanical ice sheet model: Basic sensitivity, ice stream development, and ice flow across subglacial lakes, *J. Geophys. Res.*, *108*(B8), 2382, doi:10.1029/2002JB002329.

Phillips, T., H. Rajaram, and K. Steffen (2010), Cryo-hydrologic warming: A potential mechanism for rapid thermal response of ice sheets, *Geophys. Res. Lett.*, *7*, L20503, doi:10.1029/2010GL044397.

Rignot, E., and J. Mouginot (2012), Ice flow in Greenland for the International Polar Year 2008–2009, *Geophys. Res. Lett.*, *39*, L11501, doi:10.1029/2012GL051634.

Seroussi, H., M. Morlighem, E. Rignot, A. Khazendar, E. Larour, and J. Mouginot (2013), Dependence of century-scale projections of the Greenland ice sheet on its thermal regime, *J. Glaciol.*, *59*(218), 1024–1034, doi:10.3189/2013JoG13J054.

Seroussi, H., M. Morlighem, E. Larour, E. Rignot, and A. Khazendar (2014), Hydrostatic grounding line parameterization in ice sheet models, *Cryosphere*, *8*(6), 2075–2087, doi:10.5194/tc-8-2075-2014.

Shapero, D. R., I. R. Joughin, K. Poinar, M. Morlighem, and F. Gillet-Chaulet (2016), Basal resistance for three of the largest Greenland outlet glaciers, *J. Geophys. Res. Earth Surf.*, *121*, 168–180, doi:10.1002/2015JF003643.

Shapiro, N., and M. Ritzwoller (2004), Inferring surface heat flux distributions guided by a global seismic model: Particular application to Antarctica, *Earth Planet. Sci. Lett.*, *223*(1–2), 213–224, doi:10.1016/j.epsl.2004.04.011.

Sohn, H., K. Jezek, and C. van der Veen (1998), Jakobshavn Glacier, West Greenland: 30 years of spaceborne observations, *Geophys. Res. Lett.*, *25*(14), 2699–2702, doi:10.1029/98GL01973.

Thomas, R. (2004), Force-perturbation analysis of recent thinning and acceleration of Jakobshavn Isbrae, Greenland, *J. Glaciol.*, *50*(168), 57–66, doi:10.3189/172756504781830321.

Truffer, M., and K. Echelmeyer (2003), Of isbræ and ice streams, *Ann. Glaciol.*, *36*, 66–72, doi:10.3189/172756403781816347.

van der Veen, C. J., J. C. Plummer, and L. A. Stearns (2011), Controls on the recent speed-up of Jakobshavn Isbræ, West Greenland, *J. Glaciol.*, *57*(204), 770–782.

Vieli, A., and F. Nick (2011), Understanding and modelling rapid dynamic changes of tidewater outlet glaciers: Issues and implications, *Surv. Geophys.*, *32*(4–5), 437–458.